ACS APPLIED MATERIALS & INTERFACES

Research Article

Cite This: ACS Appl. Mater. Interfaces 2020, 12, 1412−1418

www.acsami.org

Metal−Organic Frameworks with Double Channels for Rapid and Reversible Adsorption of 1,2-Ethylenediamine and Gases

Mao-Long Chen,[†,‡] Yan-Ying Feng,[‡] Si-Yuan Wang,[†] Yun-Hui Cheng,[‡] and Zhao-Hui Zhou*[,†]

[†]State Key Laboratory of Physical Chemistry of Solid Surfaces, College of Chemistry and Chemical Engineering, Xiamen University, Xiamen 361005, China

[‡]College of Chemistry and Food Engineering, Changsha University of Science & Technology, Changsha 410114, China

Supporting Information

ABSTRACT: Selective liquid and gas adsorptions are important for environmental control and industrial processes. Here, unique porous lanthanide−organic frameworks of $[Ln_2(1,3\text{-pdta})_2(H_2O)_2]_n^{2n-}$ {Ln = La (**1**), Ce (**2**), Pr (**3**), and Nd (**4**), 1,3-pdta = $CH_2[CH_2N(CH_2CO_2H)_2]_2$} are template-synthesized by 1,2-ethylenediamine and fully characterized, which possess hydrophobic and hydrophilic open channels simultaneously. The skeletons are stable up to 200 °C. Obvious downfield shifts have been observed for 1,2-ethylenediamine in the confined channel with solid-state ^{13}C NMR measurement. The ammonium salt is directly used for the removal of 1,2-ethylenediamine in water. Its saturated adsorption capacity is reached in <1 min and can be regenerated easily with a similar uptake capacity. Moreover, the materials can also selectively adsorb O_2, CH_4, and CO_2, respectively, which is useful for CO_2/CH_4, CO_2/H_2, and O_2/N_2 separation. The combined hydrophobic and hydrophilic open channels of the lanthanides make them promising functional materials for the elimination of 1,2-ethylenediamine and gas separations.

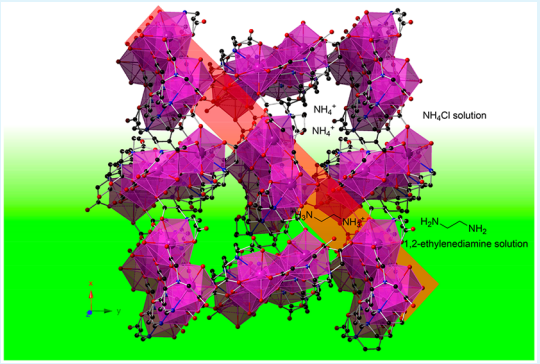

KEYWORDS: *metal−organic frameworks, 1,2-ethylenediamine, adsorption, 1,3-propanediaminetetraacetic acid, ion exchange, gas adsorption, double channels*

INTRODUCTION

Porous metal−organic frameworks (MOFs) have state-of-the-art applications in many fields, such as adsorption and separation,[1−3] chemical sensors,[4−6] catalysts,[7−9] magnetic materials, and luminescent materials.[10,11] MOF materials can be designed and synthesized using appropriate ligands and open metal sites. Although many organic ligands, such as 1,3,5-tris(4-carboxyphenyl)benzene, benzene-1,3,5-tricarboxylic acid, and benzene-1,4-dicarboxylic acid, are used to construct the most known porous MOFs,[12,13] the search for more ligands to construct new MOFs with different properties for new applications has continued. During this process, some ionic MOFs are constructed.[14−17] Their ion-exchange properties have attracted much interest with respect to capture of diverse corrosive and/or toxic cationic and anionic species.[18−21]

In another aspect, 1,2-ethylenediamine readily reacts with the moisture in humid air to produce a corrosive, toxic, and irritating mist, to which even short exposure can cause serious health damage.[22,23] Thus, rapidly removing 1,2-ethylenediamine from water is of significance in terms of environmental protection. Some researchers have eliminated 1,2-ethylenediamine and other nitrogen-containing organic compounds in wastewater by oxidizing them to harmless gases.[24] In this method, the wastewater needs to be gasified into waste gas in a heated space, which is a high energy consumption process. Azeotropic distillation using 1,2-dichloroethane as an entrainer has also beens proposed for separation of ethylenediamine from water.[25] Ethylenediamine can then be removed from the wastewater in an electrolyte solution with addition of polyaluminum sulfate.[23] Many studies have grafted 1,2-ethylenediamine onto porous materials for selective adsorption of CO_2 from mixed gases.[26−29] One study also modified a zeolite with 1,2-ethylenediamine for sorption of Th(IV).[30] However, reversible adsorption of 1,2-ethylenediamine has not been reported.

It is noted that ion exchange offers solutions to many concurrent problems in both environmental and energy related regulations.[31] In this study, we developed a novel material to achieve the goal of removing 1,2-ethylenediamine from water using lanthanide metal−organic frameworks, where $[Ln_2(1,3\text{-pdta})_2(H_2O)_2]_n^{2n-}$ (Ln = La, Ce, Pr, and Nd, 1,3-pdta = $CH_2[CH_2N(CH_2CO_2H)_2]_2$) MOFs possessing two types of open channels have been isolated from the reactions of the \lanthanide and 1,3-propanediaminetetraacetate that show rapid and reversible adsorption of 1,2-ethylenediamine and CO_2 and O_2 gases.

Received: November 7, 2019
Accepted: December 16, 2019
Published: December 16, 2019

DOI: 10.1021/acsami.9b20184
ACS Appl. Mater. Interfaces 2020, 12, 1412−1418

RESULTS AND DISCUSSION

Syntheses. Colorful crystals of $(H_2en)_n[Ln_2(1,3\text{-pdta})_2(H_2O)_2]_n{\cdot}5nH_2O$ [Ln = La (**1**), Ce (**2**), Pr, (**3**), and Nd (**4**)] were synthesized by the reactions of $LnCl_3$ and 1,3-H_4pdta templated by 1,2-ethylenediamine in good yields, where $[H_2en]^{2+}$ in **1** can be exchanged with $[NH_4]^+$ for the preparation of $(NH_4)_{2n}[La_2(1,3\text{-pdta})_2(H_2O)_2]_n{\cdot}4.5nH_2O$ (**1a**). However, trigonal colorless crystalline solids were mostly obtained, as reported for a similar reaction without a template.[32] The pH value and countercations are very important for isolating the different products, such as dimeric complexes[33] and trigonal[32] and tetragonal crystalline solids from the reactions of $LnCl_3{\cdot}7H_2O$ and 1,3-H_4pdta in water.

Structural Analyses of the MOFs. The La^{3+} ions are decacoordinated to the four carboxyl oxygen atoms and two nitrogen atoms of one 1,3-pdta ligand, three oxygen atoms from two neighboring 1,3-pdta ligands, and one coordinated water molecule. This makes it form a dimeric unit, as shown in Figure 1a. The bridged O8 atom makes these dimeric units further extend to a two-dimensional (2D) coordination network. As shown in Figure 1b, the framework contains two different types of channels. The structure with only the bridged atoms and lanthanum ions clearly shows the two types of channels (Figure 1c).

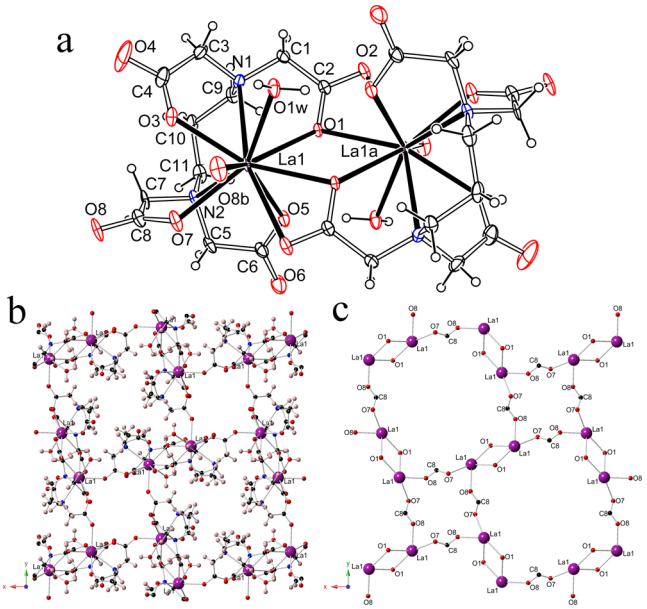

Figure 1. Crystal structure of **1**. (a) Ortep diagram of the $[La_2(1,3\text{-pdta})_2(H_2O)_2]^{2-}$ dimeric unit. (b) Extended 2D coordination network of $[La_2(1,3\text{-pdta})_2(H_2O)_2]_n^{2n-}$ possessing two types of channels. (c) Structure of the framework with only the bridged atoms and lanthanum ions clearly showing the two types of channels.

A comparison of the network structures of **1** and **1a** is shown in Figure 2. **1a** possesses two different types of two-dimensional (2D) channels with cross-diameters of approximately 5.97 and 4.63 Å, respectively, which are constructed of octanuclear and tetranuclear lanthanides, respectively. If the Ln-pdta mononuclear units are considered to be nodes in the topology, the network can be simplified as a Shubnikov plane net topological motif with a Schlafli symbol of $(4{\cdot}8^2)$, as shown in Figure S1. All of the lanthanide crystals have similar cell parameters and the same space group (Table S1). The overall void space of **1a** is 870.6 Å^3 (23.2%). Although lanthanide

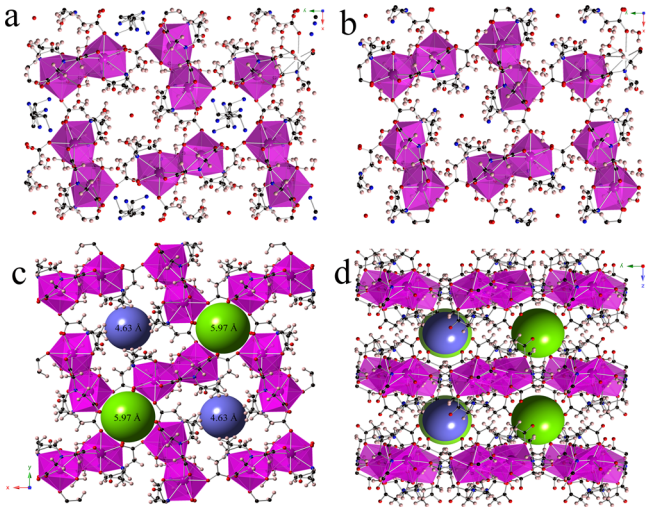

Figure 2. Comparison of the networks in **1** and **1a**. Here, one channel is surrounded by the methylene groups of the 1,3-pdta ligand (the hydrophobic channel), whereas the other channel is surrounded by carboxyl groups (the hydrophilic channel). (a) **1** with the hydrophobic channels filled with crystalline water molecules and the hydrophilic channels filled with water molecules and H_2en cations. (b) **1a** with the hydrophobic channels filled with ammonium ions and crystalline water molecules and the hydrophilic channels filled only with water molecules. (c) Diameters of the two open channels viewed along the *c* direction. (d) Channels viewed along the *a* direction.

contraction affects the cell volumes, the overall void spaces of **2** (Ce), **3** (Pr), and **4** (Nd) show different effects. The spaces of **1** (La), **2** (Ce), **3** (Pr), and **4** (Nd) calculated by PLATON[34] are 880.5 (23.3%), 852.2 (22.7%), 875.3 (23.4%), and 890.2 Å^3 (23.8%), respectively.

The calculated theoretical bond valences of the lanthanides (from the coordination bonds in Table S2) are 3.137, 3.146, 3.190, 3.126, and 2.993 for **1a** and **1**−**4**, respectively. Comparisons of selected bond distances (Å) for lanthanide 1,3-pdta, and 1,3-dpta−OH (H_4dpta−OH = 1,3-diamino-2-hydroxypropane-*N*,*N*,*N*′,*N*′-tetraacetic acid) are given in Table S3. Considering the charge balance of the framework, the charge numbers of these frameworks are estimated to be negative, so there must be countercations in the cavities. All of the H_2en-templated crystals of **1**−**4** have H_2en cations in the hydrophilic channels, as shown in Figure 2a and Figures S2−S4, respectively. However, for **1a**, there are ammonium ions in the hydrophobic channels, while the hydrophilic channels are filled with crystalline water molecules (Figure 2b). These phenomena in the ion-exchange processes are very unusual compared to those of the most reported ion-exchange processes, which always occur at the same position.[31,35−37] The overall result is that the cation charges in the open channels are transferred from one channel to another channel when $[NH_4]^+$ exchanges with $[H_2en]^{2+}$. As shown in Figure 2c,d, the two types of channels are not completely separated. This may help the cations transfer from one channel to another channel by a proton-transfer process.

Adsorption of 1,2-Ethylenediamine. Owing to $[NH_4]^+$ being exchangeable with $[H_2en]^{2+}$, we have tried to use **1a** to remove $[H_2en]^{2+}$ from water. Thus, the adsorption isotherm was recorded to estimate the maximum adsorption capacity of **1a** by varying the initial concentrations of 1,2-ethylenediamine from 5.0 to 50 mg·L^{-1} in aqueous solution (Figure 3a). With increasing initial concentration of 1,2-ethylenediamine, the

DOI: 10.1021/acsami.9b20184
ACS Appl. Mater. Interfaces 2020, 12, 1412−1418

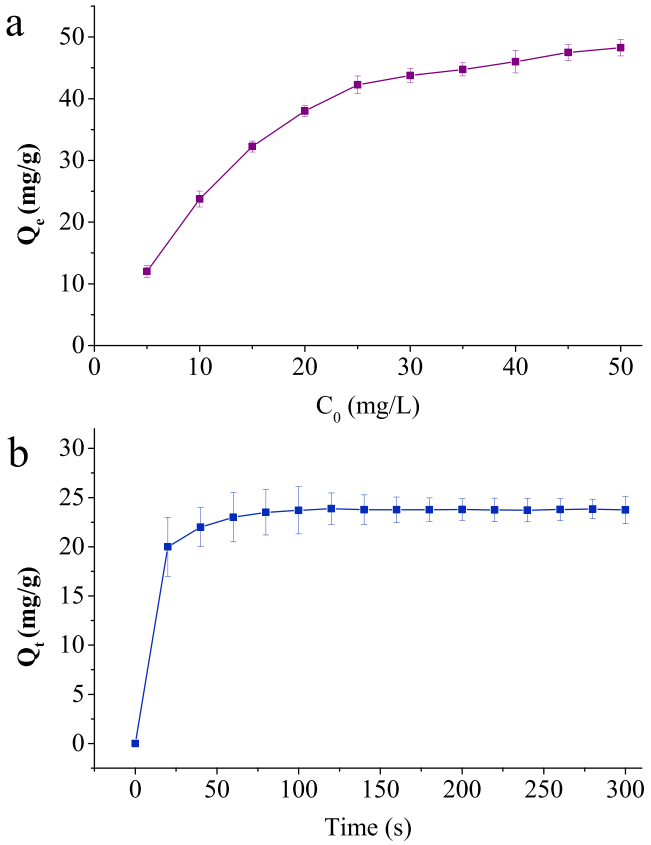

Figure 3. Adsorption properties of **1a**. (a) Adsorption isotherm of 1,2-ethylenediamine in **1a**. (b) Change of adsorption of **1a** with time for an initial 1,2-ethylenediamine concentration of 10 mg L^{-1}.

adsorbed amount of 1,2-ethylenediamine increases until reaching a plateau at ~43 mg·g^{-1}, indicating saturated adsorption. The rate of 1,2-ethylenediamine removal from water was further evaluated by monitoring the decrease in its concentration at given time intervals after immersing **1a** in 1,2-ethylenediamine solution. Adsorption reaches equilibrium within 1 min (Figure 3b), indicating fast adsorption dynamics. Adsorption isotherm and kinetic lines of **2a**–**4a** were shown in Figures S5–S7, respectively. **2a**, **3a**, and **4a** show similar results to **1a**. Finally, the reproducibility of adsorption for 1,2-ethylenediamine to **1a** was investigated. The 1,2-ethylenediamine-saturated sample was washed with 2.0 mol·L^{-1} NH_4Cl aqueous solution to obtain the regenerated sample. The adsorption capacity of **1a** for 1,2-ethylenediamine was determined again. The regenerated sample shows a similar uptake capacity to the original sample (Figure S8). We also measured the pH value of the solution in the adsorption process (Figure S9). The pH value decreases during the adsorption process, which is consistent with the pK_b values of en (4.07) and NH_3·H_2O (4.75).[38,39]

Isotherms and Kinetics of 1,2-Ethylenediamine Adsorption. To better understand the influencing factors on the adsorption process, evaluation of reaction kinetics and isotherms are necessary. The kinetics analysis is useful in predicting the adsorption rate. It is also important in designing and modeling of the adsorption process.[40] Figures S10–S13 and Table 1 show the results of kinetics and isotherm models. Among the studied models, the highest coefficient was related to the pseudo-second-order and Langmuir models.[41] The results showed that the rate of 1,2-ethylenediamine adsorption

Table 1. Kinetics and Isotherm Data of 1,2-Ethylenediamine Adsorption

	pseudo-first-order			pseudo-second-order		
kinetics data	Q_e (mg/g)	k_1 (s^{-1})	R^2	Q_e (mg/g)	k_2 (g·mg^{-1}·s^{-1})	R^2
1a	1.05	0.0092	0.434	24.39	0.017	0.999
2a	5.25	0.0104	0.465	24.27	0.0045	0.998
3a	3.92	0.0094	0.263	23.64	0.0056	0.997
4a	5.44	0.0073	0.368	24.10	0.0031	0.994
	Freundlich model			Langmuir model		
isotherms data	K_F	n	R^2	Q_m (mg/g)	K_L	R^2
1a	23.383	4.184	0.888	50.00	0.9524	0.998
2a	19.371	3.270	0.892	50.50	0.5875	0.998
3a	18.390	3.278	0.635	50.25	0.4317	0.989
4a	11.787	2.217	0.676	53.45	0.2159	0.968

was very fast. The rate of the adsorption process depends on the structural properties of MOFs (i.e., porosity, specific area, and particle size), the properties and concentrations of 1,2-ethylenediamine, and the interactions between 1,2-ethylenediamine and active sites of MOFs. Between the isotherm models data, the highest R^2 was related to the Langmuir model. According to this model, the maximum adsorption capacities of 1,2-ethylenediamine on **1a**–**4a** were 50.00, 50.50, 50.25, and 53.45 mg/g, respectively.

Adsorptions of O_2 and CO_2. Furthermore, lanthanum MOFs have been used for the gas adsorptions of O_2, CO_2, CH_4, N_2, and H_2 at 298 K, respectively, as shown in Figure 4, to probe the properties of different channels in **1** and **1a**. From the structural analysis, we know the cations of **1** and **1a** may exist in different channels. We hope that the gas adsorption results may show some indirect evidence. Low-temperature N_2 isotherms were obtained. The results show that **1** and **1a** exhibit a type-III isotherm (Figure S14) with micropores, and the BET surface area of **1** and **1a** are 1.8582 and 1.6335 m^2/g, respectively. The highest adsorption values are 10.4 and 4.1 $cm^3·g^{-1}$ (N_2). The total pore volumes of **1** and **1a** are small. In Figure 4, the biogases O_2 and CO_2 can be selectively adsorbed. As the pressure increases, the amounts of adsorbed O_2 and CO_2 gradually increase, respectively. For **1** with hydrophobic channels, the amount of adsorbed O_2 increases from 1.23 mg/g at 1.9 bar to 14.75 mg/g at 29.9 bar, and that of CO_2 increases from 2.31 mg/g at 1.9 bar to 8.79 mg/g at 29.9 bar. When $(NH_4)^+$ in the hydrophobic channels displaces $(H_2en)^{2+}$ in the hydrophilic channels, the hydrophilic channels with diameters of 5.97 Å in **1a** are exposed. As the pressure increases, the amounts of adsorbed O_2 and CO_2 also gradually increase. For **1a**, the amount of adsorbed O_2 increases from 1.74 mg/g at 1.9 bar to 20.72 mg/g at 29.9 bar, and that of CO_2 increases from 3.71 mg/g at 1.9 bar to 14.92 mg/g at 29.9 bar. The channels with larger diameters adsorb much more O_2 and CO_2 with a small amount of N_2. The small adsorption amount of N_2 is consistent with the results of low-temperature N_2 isotherms. The special hydrophobicity in **1** also allows the channels to adsorb a small amount of CH_4 (1.3 mg/g at 29.9 bar). Both channels in **1** and **1a** show no H_2 adsorption. From these data, we can conclude that **1** can be used to separate H_2/CO_2 and O_2/N_2, and **1a** can be used to separate CH_4/H_2. Separation of CO_2 and H_2 is important in water–gas shift and steam-reforming hydrogen production.[16,40] It can be inferred that both **1** and **1a** show much higher O_2 and CO_2 adsorption

DOI: 10.1021/acsami.9b20184
ACS Appl. Mater. Interfaces 2020, 12, 1412–1418

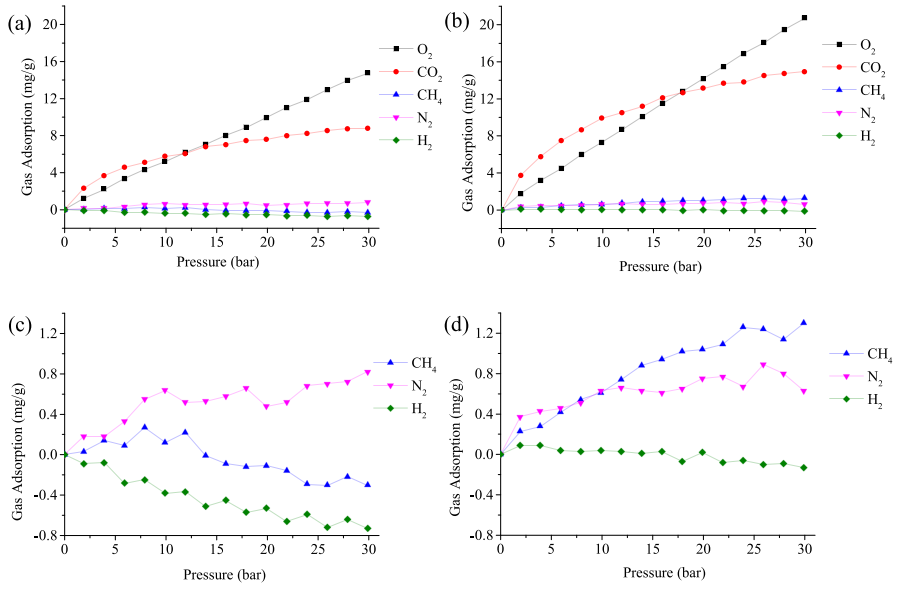

Figure 4. O_2, CO_2, CH_4, N_2, and H_2 adsorption isotherms of **1** (a) and **1a** (b) at 298 K, respectively. (c) and (d) were isotherms in (a) and (b) plotted without O_2 and CO_2, respectively.

capacities than those of H_2, N_2, and CH_4, which can be attributed to the strong interactions with the groups in porous structures. Moreover, different hydrophobic and hydrophilic channels could influence the O_2 and CO_2 adsorption capacities, which cause **1a** with hydrophilic channels (5.97 Å) showing higher adsorption amounts of O_2 and CO_2 than those of **1** with the hydrophobic channels (4.63 Å).[28]

NMR and Infrared (IR) Spectroscopic Analyses. To verify the nanoscale effects of the open channels, we have performed solid-state ^{13}C NMR (Figure 5) and IR (Figure 6 and Figure S8) spectroscopies of **1** and **1a**, respectively. The chemical shifts are listed in Table S4. In a comparison with the spectra of **1** and **1a**, the new peak at 38.3 ppm for **1** can be ascribed to the methylene groups of 1,2-ethylenediamine in the hydrophilic channel, which shows a clear downfield shift compared to those of acidic 1,2-ethylenediamine dihydro-

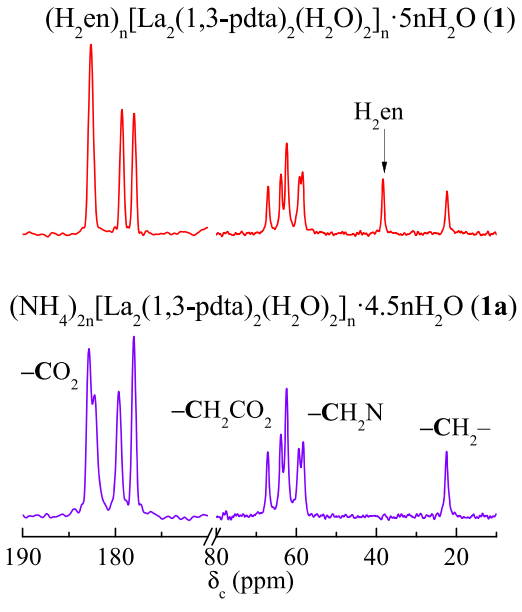

Figure 5. Solid-state ^{13}C NMR spectra of solids **1** and **1a**.

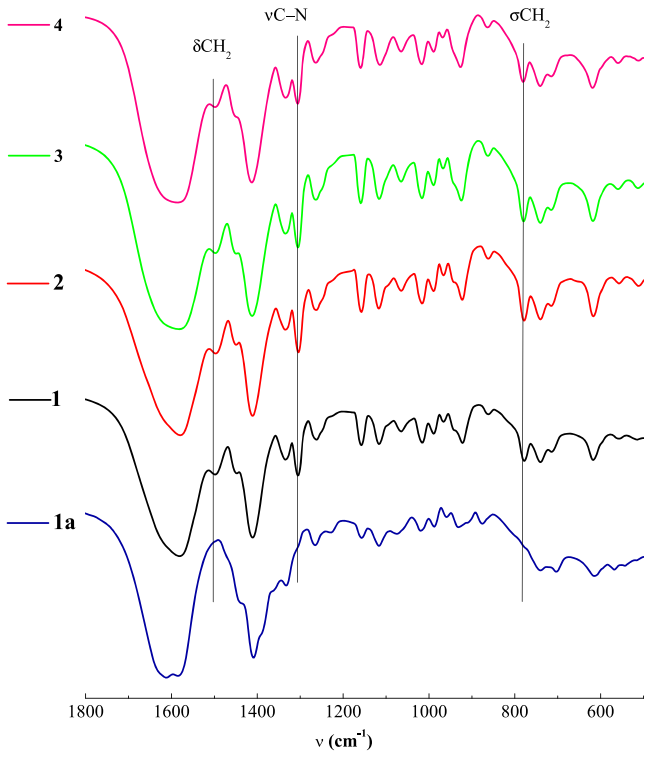

Figure 6. IR spectra of **1a** and **1**–**4** in the range 500–1800 cm^{-1}.

chloride (37.4 ppm) and sulfate (37.5 ppm),[42] indicating the nanoscale effect in the confined channel. The IR spectra of **1**–**4** (Figure 6) show three clear peaks at 1498, 1306, and 779 cm^{-1}, which can be attributed to ν_{C-H}, ν_{C-N}, and ν_{C-H}, respectively. In a comparison of these new absorption peaks with those of 1,2-ethylenediamine, 1,2-ethylenediamine hydrochloride, and 1,2-ethylenediamine sulfate (Table S5), there is a clear red shift for ν_{C-H}, which also indicates the nanoscale effect in the confined channel. Thermogravimetric analysis was also performed to characterize the materials (Figure S9), which indicates that **1**–**4** and **1a** are stable and maintain their

DOI: 10.1021/acsami.9b20184
ACS Appl. Mater. Interfaces 2020, 12, 1412–1418

integrities of the skeleton structures up to 200 °C. The differential scanning calorimetry (DSC) curves of **1** and **1a** are also shown in Figure S9b. The DSC curves are quite different, which indicate the cations exiting in different channels may cause some differences in heat flows. The photoluminescence spectra (Figure S10) show large differences between **1** and **1a**, which indicate the effects of guest molecules and counterions in the MOF materials.[43]

CONCLUSION

In summary, we have developed a new type of lanthanide chelates with two different open channels. Owing to the unique hydrophobic and hydrophilic properties of the open channels, the interaction between the framework and the guest molecules or countercations can be used for rapid and reversible adsorptions of 1,2-ethylenediamine and the gases of O_2 and CO_2. Ion exchange and gas adsorptions between the hydrophobic and hydrophilic channels will be useful for the design and synthesis of new framework−guest hybrid materials with unique properties.

EXPERIMENTAL SECTION

Preparation of $(H_2en)_n[La_2(1,3\text{-pdta})_2(H_2O)_2]_n{\cdot}5nH_2O$ (1). The reagents are from Sigma. 1,3-Propanediaminetetraacetic acid (0.613 g, 2.0 mmol), 1,2-ethylenediamine (0.55 mL), and $LaCl_3{\cdot}7H_2O$ (0.743 g, 2.0 mmol) were dissolved in water (15 mL). The mixture was heated at 70 °C for 1 day. The tetragonal colorless crystalline materials were separated from the evaporated solution, washed with cold water and ethanol, and then dried under vacuum. The yield was 78.5% (0.841 g). Found (calcd for $C_{24}H_{52}N_6O_{23}La_2$): C, 26.57 (26.93); H, 4.78 (4.90); N, 8.05 (7.85). IR (KBr disk, cm^{-1}): 3421_{vs}, 2961_s, 2853_s, $\nu_{as}(CO_2)$, 1581_{vs}, 1500_m; $\nu_s(CO_2)$, 1449_m, 1411_{vs}, 1334_m, 1305_m, 1262_w, 1158_w, 1116_m, 1065_w, 1016_w, 989_w, 966_w, 922_m, 861_w, 778_m, 740_m, 711_m, 617_m, 555_m, 517_w, 431_m.

Preparations of $(H_2en)_n[Ln_2(1,3\text{-pdta})_2(H_2O)_2]_n{\cdot}5nH_2O$ [Ln = Ce (2), Pr (3), and Nd (4)]. 1,3-Propanediaminetetraacetic acid (0.613 g, 2.0 mmol) and $CeCl_3{\cdot}7H_2O$ (0.744 g, 2.0 mmol) were dissolved in water (15 mL). The pH value of the mixture was adjusted to ~6.5 by 1,2-ethylenediamine. The mixture was heated at 70 °C for 1 day. The tetragonal colorless crystalline materials were separated from the evaporated solution, washed with cold water and ethanol, and then dried under vacuum. The yield of **2** was 82.0% (0.882 g). Found (calcd for $C_{24}H_{52}N_6O_{23}Ce_2$): C, 26.77 (26.87); H, 4.68 (4.88); N, 7.95 (7.83). IR (KBr disk, cm^{-1}): 3423_{vs}, 2960_s, 2856_s, $\nu_{as}(CO_2)$, 1579_{vs}, 1495_m; $\nu_s(CO_2)$, 1447_m, 1411_{vs}, 1335_m, 1304_m, 1263_w, 1158_w, 1117_m, 1065_w, 1016_w, 989_w, 966_w, 923_m, 862_w, 778_m, 741_m, 711_m, 617_m, 556_m, 512_w, 438_m. When $PrCl_3{\cdot}7H_2O$ was used instead of $CeCl_3{\cdot}7H_2O$, the yield of **3** was 83.7% (0.901 g). Found (calcd for $C_{24}H_{52}N_6O_{23}Pr_2$): C, 26.97 (26.83); H, 4.98 (4.88); N, 7.75 (7.82). IR (KBr disk, cm^{-1}): 3419_{vs}, 2961_s, 2851_s, $\nu_{as}(CO_2)$, 1581_{vs}, 1495_m; $\nu_s(CO_2)$, 1447_m, 1412_{vs}, 1335_m, 1305_m, 1264_w, 1159_w, 1116_m, 1065_w, 1016_w, 989_w, 967_w, 925_m, 863_w, 780_m, 741_m, 717_m, 618_m, 561_m, 513_w, 440_m. When $NdCl_3{\cdot}7H_2O$ was used instead of $CeCl_3{\cdot}7H_2O$, the yield of **4** was 90.6% (0.980 g). Found (calcd for $C_{24}H_{52}N_6O_{23}Nd_2$): C, 26.75 (26.66); H, 4.88 (4.85); N, 7.65 (7.77). IR (KBr disk, cm^{-1}): 3416_{vs}, 2961_s, 2856_s, $\nu_{as}(CO_2)$, 1586_{vs}, 1498_m; $\nu_s(CO_2)$, 1447_m, 1413_{vs}, 1334_m, 1306_m, 1264_w, 1159_w, 1114_m, 1065_w, 1017_w, 989_w, 969_w, 927_m, 867_w, 781_m, 741_m, 717_m, 619_m, 564_m, 513_w, 446_m.

Preparation of $(NH_4)_{2n}[La_2(1,3\text{-pdta})_2(H_2O)_2]_n{\cdot}4.5nH_2O$ (1a). **1a** was obtained by immersing crystalline solid **1** (1.071g, 1.0 mmol) in NH_4Cl solution (2.0 mol·L^{-1}, 30 mL) and heated at 70 °C for 1 h with high probability and yield of ~90%. Found (calcd for $C_{22}H_{49}N_6O_{22.5}La_2$): C, 25.15 (25.52); H, 4.68 (4.77); N, 8.01 (8.12). IR (KBr disk, cm^{-1}): 3443_{vs}, 3251_s, $\nu_{as}(CO_2)$, 1610_{vs}, 1581_{vs}; $\nu_s(CO_2)$, 1409_{vs}, 1331_s, 1265_w, 1224_w, 1157_w, 1116_m, 1076_w, 1019_w, 988_w, 931_w, 876_w, 740_m, 703_m, 615_m, 566_m, 477_m.

1,2-Ethylenediamine Adsorption. An ACQUITY ultraperformance liquid chromatograph and a Waters Xevo TQD mass spectrometer (UPLC−MS/MS, Waters Co., USA) were used for 1,2-ethylenediamine analysis. The detailed quantification procedure and parameters are given in the Supporting Information. Typically, the powder of crystals of **1a** (40 mg) was dispersed in 100 mL of 1,2-ethylenediamine solution. After 5 min, the solution was separated from the adsorbent with a syringe filter and the UPLC−MS/MS system was used to analyze the residual concentration of 1,2-ethylenediamine. The 1,2-ethylenediamine adsorption efficiency was calculated by the equation

$$\text{adsorption efficiency}\ (\%) = \frac{C_0 - C_e}{C_0} \times 100\%$$

where C_0 and C_e are the initial and equilibrium 1,2-ethylenediamine concentrations (mg·L^{-1}), respectively.

To evaluate the adsorption capacity, the powder of crystals of **1a** (40 mg) was separately dispersed in 100 mL of 1,2-ethylenediamine solutions with different concentrations between 5.0 and 50 mg·L^{-1}. After 5 min, the solution was separated from the adsorbent with a syringe filter and the residual concentration of 1,2-ethylenediamine was measured. The equilibrium adsorption capacity (Q_e) was calculated by the equation

$$Q_e = \frac{C_0 - C_e}{m} V$$

where V (L) is the volume of the solution and m (g) is the mass of the sorbent.

For the adsorption kinetics experiment, the powder of crystals of **1a** (40 mg) was dispersed in 100 mL of 10 mg·L^{-1} 1,2-ethylenediamine solution, which was then stirred for a specific time at room temperature. The solution was filtered with a syringe filter and the residual concentration of 1,2-ethylenediamine was measured. The adsorption capacity (Q_t) was calculated by the equation

$$Q_t = \frac{C_0 - C_t}{m} \times V$$

where C_t (mg·L^{-1}) is the concentration of 1,2-ethylenediamine at time t (s).

Gas Adsorptions of $(H_2en)_n[La_2(1,3\text{-pdta})_2(H_2O)_2]_n{\cdot}5nH_2O$ (1) and $(NH_4)_{2n}[La_2(1,3\text{-pdta})_2(H_2O)_2]_n{\cdot}4.5nH_2O$ (1a). **1** or **1a** (0.20 g) was loaded into a magnetic suspension gravimetric sorption analyzer. The gas adsorption data were measured with the change in weight under different pressures of O_2 ($CO_2/CH_4/N_2/H_2$) inlet conditions at 298 K. Linear fits of the O_2 adsorption amounts of **1** and **1a** are shown in Figures S11 and S12, respectively. Detail adsorption data of O_2, CO_2, CH_4, N_2, and H_2 (mg/g) for **1** and **1a** at 298 K under different pressures are given in Tables S6 and S7, respectively.

Physical Measurements. All of the chemicals were of analytical- or reagent-grade purity and were used as-received. The pH value was measured with a PHB-8 digital pH meter (Shanghai Kangyi Instrument Co. Ltd., Shanghai, China) by the potentiometric method. The IR spectra were recorded as KBr disks and mulls in Nujol with a Nicolet 330 FT-IR spectrophotometer. Thermogravimetric analysis was performed with an SDT-Q600 thermal analyzer under an air flow of 100 mL·min^{-1} at a heating rate of 10 °C·min^{-1}. The solid-state ^{13}C NMR spectra were recorded with a Bruker AV 400 NMR spectrometer using cross-polarization, magic angle spinning (13 kHz), and adamantane as the reference. The fluorescence spectra were recorded with an F-7000 FL spectrophotometer. The N_2 sorption isotherms were measured at 77 K with liquid nitrogen on Micromeritics TriStar II Surface Area and Porosity Analyzer. The gas adsorption capacities of **1** and **1a** were evaluated with a magnetic suspension gravimetric sorption analyzer ISOSORP-HTGRA at 298 K under different pressures of O_2, CH_4, CO_2, N_2, and H_2.

X-ray Intensity Data. The X-ray intensity data of compounds **1**−**4** and **1a** were measured at 173(2) K with an Oxford CCD diffractometer using Mo Kα radiation (λ = 0.71073 Å). The initial model was obtained by direct methods and completion of the rest of

DOI: 10.1021/acsami.9b20184
ACS Appl. Mater. Interfaces 2020, 12, 1412−1418

the structure was achieved by difference Fourier strategies. The structures were refined by least-squares on F^2 using anisotropic displacement parameters for the non-H atoms. All of the calculations performed to solve and refine the structures were performed with SHELX-2018/3.[44,45]

■ ASSOCIATED CONTENT

Supporting Information

The Supporting Information is available free of charge at https://pubs.acs.org/doi/10.1021/acsami.9b20184.

Quantification and adsorption of 1,2-ethylenediamine, kinetics and isotherms fitting of 1,2-ethylenediamine on **1a**−**4a**, gas adsorptions (CO_2, O_2, CH_4, N_2, and H_2), additional structural details, crystallographic data (CCDC numbers are 1864371−1864375), IR spectra, thermogravimetric curves, and photoluminescence spectra (PDF)

X-ray crystallographic data (**1**) (CIF)

X-ray crystallographic data (**1a**) (CIF)

X-ray crystallographic data (**2**) (CIF)

X-ray crystallographic data (**3**) (CIF)

X-ray crystallographic data (**4**) (CIF)

■ AUTHOR INFORMATION

Corresponding Author

*E-mail: zhouzh@xmu.edu.cn.

ORCID

Zhao-Hui Zhou: 0000-0001-7271-7009

Notes

The authors declare no competing financial interest.

■ ACKNOWLEDGMENTS

This work was financially supported by the National Natural Science Foundation of China (21773196, 31601550) and Natural Science Foundation of Hunan Province (2019JJ50638).

■ REFERENCES

(1) Duan, J.; Yan, R.; Qin, L.; Wang, Y.; Wen, L.; Cheng, S.; Xu, H.; Feng, P. Highly selective gaseous and liquid-phase separation over a novel cobalt (II) metal-organic framework. *ACS Appl. Mater. Interfaces* **2018**, *10*, 23009−23017.

(2) Li, L.; Lin, R. B.; Krishna, R.; Li, H.; Xiang, S.; Wu, H.; Li, J.; Zhou, W.; Chen, B. Ethane/ethylene separation in a metal-organic framework with iron-peroxo sites. *Science* **2018**, *362*, 443−446.

(3) McGuirk, C. M.; Siegelman, R. L.; Drisdell, W. S.; Runcevski, T.; Milner, P. J.; Oktawiec, J.; Wan, L. F.; Su, G. M.; Jiang, H. Z. H.; Reed, D. A.; Gonzalez, M. I.; Prendergast, D.; Long, J. R. Cooperative adsorption of carbon disulfide in diamine-appended metal-organic frameworks. *Nat. Commun.* **2018**, *9*, 5133.

(4) Lustig, W. P.; Mukherjee, S.; Rudd, N. D.; Desai, A. V.; Li, J.; Ghosh, S. K. Metal-organic frameworks: functional luminescent and photonic materials for sensing applications. *Chem. Soc. Rev.* **2017**, *46*, 3242−3285.

(5) Wang, H.; Lustig, W. P.; Li, J. Sensing and capture of toxic and hazardous gases and vapors by metal-organic frameworks. *Chem. Soc. Rev.* **2018**, *47*, 4729−4756.

(6) Zhao, G.; Wang, Y.; Li, X.; Dong, X.; Wang, H.; Du, B.; Cao, W.; Wei, Q. Quenching electrochemiluminescence immunosensor based on resonance energy transfer between ruthenium (II) complex incorporated in the UiO-67 metal-organic framework and gold nanoparticles for insulin detection. *ACS Appl. Mater. Interfaces* **2018**, *10*, 22932−22938.

(7) Zhu, L.; Liu, X. Q.; Jiang, H. L.; Sun, L. B. Metal-organic frameworks for heterogeneous basic catalysis. *Chem. Rev.* **2017**, *117*, 8129−8176.

(8) Rogge, S. M. J.; Bavykina, A.; Hajek, J.; Garcia, H.; Olivos-Suarez, A. I.; Sepulveda-Escribano, A.; Vimont, A.; Clet, G.; Bazin, P.; Kapteijn, F.; Daturi, M.; Ramos-Fernandez, E. V.; Llabres i Xamena, F. X.; Van Speybroeck, V.; Gascon, J. Metal-organic and covalent organic frameworks as single-site catalysts. *Chem. Soc. Rev.* **2017**, *46*, 3134−3184.

(9) Yan, Z. H.; Du, M. H.; Liu, J.; Jin, S.; Wang, C.; Zhuang, G. L.; Kong, X. J.; Long, L. S.; Zheng, L. S. Photo-generated dinuclear $\{Eu(II)\}_2$ active sites for selective CO_2 reduction in a photosensitizing metal-organic framework. *Nat. Commun.* **2018**, *9*, 3353.

(10) Kurmoo, M. Magnetic metal-organic frameworks. *Chem. Soc. Rev.* **2009**, *38*, 1353−1379.

(11) Zhang, Q.; Wang, J.; Kirillov, A. M.; Dou, W.; Xu, C.; Xu, C. L.; Yang, L.; Fang, R.; Liu, W. S. Multifunctional Ln-MOF luminescent probe for efficient sensing of Fe^{3+}, Ce^{3+}, and acetone. *ACS Appl. Mater. Interfaces* **2018**, *10*, 23976−23986.

(12) Ortiz, O. L.; Ramírez, L. D. *Coordination Polymers and Metal Organic Frameworks: Properties, Types, and Applications*; Nova Science Publishers: Hauppauge, N.Y., 2012.

(13) Schröder, M. *Functional Metal-Organic Frameworks: Gas Storage, Separation, and Catalysis*; Springer: Berlin, New York, 2010.

(14) Duan, J.; Jin, W.; Kitagawa, S. Water-resistant porous coordination polymers for gas separation. *Coord. Chem. Rev.* **2017**, *332*, 48−74.

(15) Rodenas, T.; Luz, I.; Prieto, G.; Seoane, B.; Miro, H.; Corma, A.; Kapteijn, F.; Llabres i Xamena, F. X.; Gascon, J. Metal-organic framework nanosheets in polymer composite materials for gas separation. *Nat. Mater.* **2015**, *14*, 48−55.

(16) LeValley, T. L.; Richard, A. R.; Fan, M. The progress in water gas shift and steam reforming hydrogen production technologies-A review. *Int. J. Hydrogen Energy* **2014**, *39*, 16983−17000.

(17) Chen, M. L.; Tang, X.; Lu, T. H.; Zhan, X. Q.; Zhou, Z. H. Mixed-ligand lanthanide complexes constructed by flexible 1,3-propanediaminetetraacetate and rigid terephthalate. *J. Coord. Chem.* **2019**, *72*, 1547−1559.

(18) Kumar, P.; Pournara, A.; Kim, K. H.; Bansal, V.; Rapti, S.; Manos, M. J. Metal-organic frameworks: Challenges and opportunities for ion-exchange/sorption applications. *Prog. Mater. Sci.* **2017**, *86*, 25−74.

(19) Zhao, X.; Bu, X.; Wu, T.; Zheng, S. T.; Wang, L.; Feng, P. Selective anion exchange with nanogated isoreticular positive metal-organic frameworks. *Nat. Commun.* **2013**, *4*, 2344.

(20) Wright, A. M.; Rieth, A. J.; Yang, S.; Wang, E. N.; Dinca, M. Precise control of pore hydrophilicity enabled by post-synthetic cation exchange in metal-organic frameworks. *Chem. Sci.* **2018**, *9*, 3856−3859.

(21) Peng, Y.; Huang, H.; Zhang, Y.; Kang, C.; Chen, S.; Song, L.; Liu, D.; Zhong, C. A versatile MOF-based trap for heavy metal ion capture and dispersion. *Nat. Commun.* **2018**, *9*, 187.

(22) Wikipedia. Ethylenediamine. https://en.wikipedia.org/wiki/Ethylenediamine (updated: 11/19/2018; accessed: 11/28/2018).

(23) Panaitescu, C.; Jinescu, C.; Mares, A. M. Study on ethylenediamine removal from textile industry wastewater. *Rev. Chim. (Bucharest, Rom.)* **2016**, *67*, 925−928.

(24) Tsutomu, T.; Keiji, H.; Junji, O.; Mitsuaki, I.; Kunio, S., Method of treating waste water and apparatus for treating waste water using the method 2000. U.S. Patent No. US6652759.

(25) Panaitescu, C. New Method to Separate Ethylenediamine from Water-Ethylenediamine Mixture. *Rev. Chim. (Bucharest, Rom.)* **2016**, *67*, 349−352.

(26) Zhong, R. Q.; Yu, X. F.; Meng, W.; Han, S. B.; Liu, J.; Ye, Y. X.; Sun, C. Y.; Chen, G. J.; Zou, R. Q. A solvent 'squeezing' strategy to graft ethylenediamine on $Cu_3(BTC)_2$ for highly efficient CO_2/CO separation. *Chem. Eng. Sci.* **2018**, *184*, 85−92.

(27) Zhang, F. F.; Shang, H.; Yang, J. F.; Ouyang, K.; Li, J. P. Ethylenediamine modified light metal aluminum-metal-organic frame-

DOI: 10.1021/acsami.9b20184
ACS Appl. Mater. Interfaces 2020, 12, 1412−1418

work material for CO_2/CH_4 separation. *Chin. J. Inorg. Chem.* **2017**, *33*, 1611−1617.
(28) Molavi, H.; Joukani, F. A.; Shojaei, A. Ethylenediamine grafting to functionalized NH_2-UiO-66 using green aza-michael addition reaction to improve CO_2/CH_4 adsorption selectivity. *Ind. Eng. Chem. Res.* **2018**, *57*, 7030−7039.
(29) Kalantarifard, A.; Ghavaminejad, A.; Yang, G. S. High CO_2 adsorption on improved ZSM-5 zeolite porous structure modified with ethylenediamine and desorption characteristics with microwave. *J. Mater. Cycles Waste Manage.* **2017**, *19*, 394−405.
(30) Liu, P.; Wu, H. Y.; Yuan, N.; Yin, Z. X.; Pan, D. Q.; Wu, W. S. beta-Zeolite modified by ethylenediamine for sorption of Th(IV). *Radiochim. Acta* **2017**, *105*, 463−470.
(31) SenGupta, A. K. *Ion Exchange in Environmental Processes: Fundamentals, Applications and Sustainable Technology*; John Wiley & Sons, Inc.: Bethlehem, USA, 2017.
(32) Chen, M. L.; Guo, Y. C.; Yang, F.; Liang, J. X.; Cao, Z. X.; Zhou, Z. H. A lanthanum chelate possessing an open-channel framework with water nanotubes: properties and desalination. *Dalton Trans.* **2014**, *43*, 6026−6031.
(33) Chen, M. L.; Hou, Y. H.; Xia, W. S.; Weng, W. Z.; Cao, Z. X.; Zhou, Z. H.; Wan, H. L. Dimeric 1,3-propanediaminetetraacetato lanthanides as the precursors of catalysts for the oxidative coupling of methane. *Dalton Trans.* **2014**, *43*, 8690−8697.
(34) Spek, A. L. *PLATON, A Multipurpose Crystallographic Tool*. In Utrecht University: Utrecht, The Netherlands, 2008.
(35) Kim, M.; Cahill, J. F.; Fei, H.; Prather, K. A.; Cohen, S. M. Postsynthetic ligand and cation exchange in robust metal−organic frameworks. *J. Am. Chem. Soc.* **2012**, *134*, 18082−18088.
(36) Genna, D. T.; Wong-Foy, A. G.; Matzger, A. J.; Sanford, M. S. Heterogenization of homogeneous catalysts in metal-organic frameworks via cation exchange. *J. Am. Chem. Soc.* **2013**, *135*, 10586−10589.
(37) Fei, H.; Pham, C. H.; Oliver, S. R. Anion exchange of the cationic layered material $[Pb_2F_2]^{2+}$. *J. Am. Chem. Soc.* **2012**, *134*, 10729−10732.
(38) Slater, A. M. The IUPAC aqueous and non-aqueous experimental pKa data repositories of organic acids and bases. *J. Comput.-Aided Mol. Des.* **2014**, *28*, 1031−1034.
(39) Serjeant, E. P.; Dempsey, B. *Ionisation Constants of Organic Acids in Aqueous Solution*; Pergamon Press: Oxford, 1979.
(40) Platon, A.; Wang, Y. In *Hydrogen and Syngas Production and Purification Technologies*; Liu, K., Subramani, V., Eds.; Wiley: New York, 2009.
(41) Ho, Y.; Mckay, G. Pseudo-second order model for sorption processes. *Process Biochem.* **1999**, *34*, 451−465.
(42) Yamaji, T.; Saito, T.; Hayamizu, K.; Yanagisawa, M.; Yamamoto, O. *Spectral Database for Organic Compounds*; National Institute of Advanced Industrial Science and Technology (AIST). https://sdbs.db.aist.go.jp (accessed 08/06/2018).
(43) Wu, Z. F.; Gong, L. K.; Huang, X. Y. A Mg-CP with in situ encapsulated photochromic guest as sensitive fluorescence sensor for Fe^{3+}/Cr^{3+} ions and nitro-explosives. *Inorg. Chem.* **2017**, *56*, 7397−7403.
(44) Sheldrick, G. A short history of SHELX. *Acta Crystallogr., Sect. A: Found. Crystallogr.* **2008**, *64*, 112−122.
(45) Sheldrick, G. Crystal structure refinement with SHELXL. *Acta Crystallogr., Sect. C: Struct. Chem.* **2015**, *71*, 3−8.

DOI: 10.1021/acsami.9b20184
ACS Appl. Mater. Interfaces 2020, 12, 1412−1418